

Covalent Organic Networks for *in situ* Entrapment of Biomolecules with Superior Robustness and Durability

Zhenhua Wu^a, Huiting Shan^b, Yushuai Jiao^c, Shouying Huang^{c, d}, Xiaodong Wang^e,

Kang Liang^{f, *} and Jiafu Shi^{a, b, d, *}

^a *School of Environmental Science and Engineering, Tianjin University, Tianjin 300072 China*

^b *Joint School of National University of Singapore and Tianjin University International Campus of Tianjin University, Fuzhou 350207 China*

^c *Key Laboratory for Green Chemical Technology of Ministry of Education, School of Chemical Engineering and Technology, Tianjin University, Tianjin 300072 China*

^d *Collaborative Innovation Center of Chemical Science and Engineering (Tianjin), Tianjin 300072, China*

^e *Chemical and Materials Engineering, School of Engineering, University of Aberdeen, Aberdeen AB24 3UE, Scotland, United Kingdom*

Chemical Engineering, Department of Engineering, Lancaster University, Lancaster LA1 4YW, United Kingdom

^f *School of Chemical Engineering, Graduate School of Biomedical Engineering and Australian Centre for NanoMedicine University of New South Wales, Sydney, New South Wales 2052, Australia*

** Corresponding author: kang.liang@unsw.edu.au (K. Liang); shijiafu@tju.edu.cn (J. Shi)*

Abstract

Enzyme-based nanobiohybrids (EnNBHs) are an emerging biocatalyst family that can manufacture industrial products such as biofuels and biochemical in a green and low-carbon manner. Designing high-performance EnNBHs can confer the enzymes with superior robustness and durability, while current strategies confront grand challenges. Herein, a facile and versatile *in situ* entrapment strategy is developed to entrap a series of enzymes in imine-based covalent organic networks (CONs) under mild conditions. Enzymes can promote the nucleation and growth of CONs while the CONs coating can act as a protection layer for the enzymes. The external CONs can safeguard the hosted biomolecules from being denatured under unfavorable conditions, such as high temperature, strong acidic/basic conditions, organic solvents, etc. Given the short-range ordered open porous structure, CONs can offer rapid transport channels for substrates and products, exhibiting superior catalytic efficiency. Furthermore, CONs can be endowed with biofunctionality and serve as a cell-mimic nanoreactor for multienzyme catalysis, demonstrating great potentials in biomedicine, biosensing and so on.

Keywords: Enzyme-based Nanobiohybrids; Biomolecules; Entrapment; Covalent Organic Networks; Biocatalysis

1. Introduction

Enzymes are active biomolecules that can catalyze a series of chemical reactions under ambient conditions and play dominant roles in cell metabolisms [1]. *In vitro* application of enzyme catalysis is rather attractive and has become a powerful platform for chemical transformation, while being restricted by intrinsic low stability and durability of enzymes [2]. Enzyme-based nanobiohybrids (EnNBHs) by integrating the library of synthetic materials and the database of

gene-encoded enzyme have become an emerging candidate for conferring enzymes with superior robustness and durability [3, 4]. Meanwhile, the enzymes can impart biofunctions to the host synthetic materials. Thus, the construction of high-performance EnNBHs is of great importance and highly desirable [4, 5].

In the past decades, tremendous efforts have been devoted to exploring synthetic materials including polymers, silica, and metal oxides, and so on for the construction of EnNBHs [6]. Amongst, reticular network nanomaterials (including metal-organic frameworks (MOFs), covalent organic frameworks (COFs), and hydrogen-bond frameworks (HOFs)) with ordered structural skeletons and permanent porosity have already utilized as good candidates for constructing various EnNBHs [7-9]. Especially, MOFs formed by coordination bond between metal nodes and organic ligands have sparked great interests for the construction of EnNBHs via *in situ* enzyme entrapment [7, 10, 11]. Particularly, zeolitic imidazolate frameworks (ZIFs) with good biocompatibility, low cytotoxicity and mild synthesis condition have been widely utilized for the construction of EnNBHs [12-15]. However, the small pore apertures (<2 nm) [16], and instability of ZIFs severely limit their applications in biotransformation [17]. Various strategies including linker labilization [18], surface-protected etching [19, 20], and competitive coordination of modulators [21-23], have been employed to enlarge voids or generate defects in intrinsic structure of MOFs to accelerate the diffusion rate of reactants [24]. While excessive voids or defects may aggravate to amorphization or even decompose MOFs caused by chelating agents [25], acidic pH [17, 26], light [27], and so on [11]. Alternatively, COFs with strong organic covalent bonds may be another excellent candidate for building high-efficiency EnNBHs [28]. While COFs are commonly prepared under the conditions of organic solvent and high temperature [29, 30], which are unfavorable or abiotic for biomolecules, thus resulting in the inactivation of enzymes during *in situ* entrapment process. Given the above features, COFs have been adopted to immobilize enzymes through direct physical adsorption, which may narrow the

pore apertures and thereby increase mass transfer resistance [31-33]. In this regard, reticular network nanomaterials with ease of preparation, larger pore apertures and intrinsically structural stability for the construction of EnNBHs *in situ* were still urgently pursued [34-36].

Covalent organic networks (CONs) that formed through strong covalent bonds were known as a class of organic network nanomaterials with well-defined topology, tunable pore apertures, intrinsically structural stability against pH range [37, 38]. The strong covalent bonds render CONs comparable stability to COFs [39]. The formation of CONs did not require the correction and reorganization of covalent bonds, which significantly shortened the formation time of CONs by contrast with COFs [40, 41]. More importantly, compared with harsh conditions for preparation of COFs, the preparation process of CONs was compatibility to biomolecules (protein, DNA, and enzyme etc.). Given the above notable features, the CONs could offer an excellent nanomaterials candidate for the construction of advanced EnNBHs.

Here, we reported a facile and versatile *de novo* strategy to construct EnNBHs through *in situ* entrapment of enzymes in CONs under ambient conditions with enhanced robustness and durability of enzymes. As shown in **Fig. 1(a)**, GOx as the model enzyme and CONs-TpBD (labelled as TpBD) as the model matrix were applied to construct the CONs-based EnNBHs (labelled as GOx@TpBD). Polyvinyl pyrrolidone (PVP) was used to disperse and stabilize enzymes during the entrapment process, and introduce abundant amino, hydroxyl and carbonyl groups on the surfaces of enzymes [13, 42]. The functional groups were capable to trigger the formation of CONs through self-assembly. The CONs coating could then act as a shielding layer and safeguard the entrapped enzymes from being denatured against high temperature, organic solvents, and various inhibitors, leading to ~ 70% retention of their initial enzyme activity. In contrast, the free enzymes lose most of their initial enzyme activity under similar conditions. Furthermore, the hierarchically porous CONs allowed improved access of substrates to the entrapped enzymes. The catalytic efficiency was thus significantly elevated by 1.35-folds

compared with enzyme@ZIFs. The CONs were further applied for entrapping dual enzymes glucose oxidase/horseradish peroxidase (GOx/HRP), which served as a cell-mimic system for multienzyme catalysis.

2. Materials and methods

2.1. Materials

Glucose oxidase from *Aspergillus Niger* (GOx, EC 1.1.3.4), D-(+)-glucose, dimethylformamide (DMF, 99.9%), 2-amino-2-(hydroxymethyl)-1, 3-propanediol (Trizma base, 99.9%), and 3, 3', 5, 5'-tetramethylbenzidine (TMB, >99.8%) were obtained from Sigma-Aldrich (St. Louis, U.S.A.). 4, 4'-Diaminobiphenyl (BD, ≥98%), p-phenylenediamine (Pa, ≥97%), acetic acid (>99.7%), hydrogen peroxide (H₂O₂, 30% wt.), sodium phosphate dibasic dodecahydrate (Na₂HPO₄·12H₂O, 99%), Zinc nitrate hexahydrate (Zn(NO₃)₂·6H₂O, 99%), sodium phosphate monobasic dihydrate (NaH₂PO₄·2H₂O, 99%) were purchased from Aladdin Industrial Corporation (Shanghai, China). Sodium acetate trihydrate, ethanol (≥99.7%), ethylene glycol (AR), chloroplatinic acid, hexane (97.0%), and acetone (≥99.5%) were obtained from Tianjin Kermel Chemical Reagent Co., Ltd. Coomassie brilliant blue (G-250), catalase (CAT, EC 1.11.1.6) was obtained from Beijing Dingguo (Beijing, China). Polyvinylpyrrolidone (PVP, MW 40000), horseradish peroxidase (HRP, > 300 U/mg), and sodium hydroxide (≥96.0%) were purchased from Shanghai YuanYe Biology Corporation (Shanghai, China). 2, 4, 6-trihydroxy-1, 3, 5-benzenetricarbaldehyde (Tp) was obtained from Jilin China Science and Technology Co., Ltd. (Jilin, China). Bovine serum albumin (BSA, ≥98%) was purchased from Amresco (Radnor, USA). Coumarin (≥99%) was obtained from Tianjin Seans Biochemical Technology Co., Ltd. 2-Methylimidazole (2-MI, ≥99.5%) was purchased from Tokyo Chemical Industry Co., Ltd. (Tokyo, Japan). All other reagents were purchased from Aladdin Industrial Corporation (Shanghai, China) and used without further purification.

2.2. Methods

2.2.1. Synthesis of EnNBHs

The synthesis of GOx@TpBD was described detailedly as follows: the 50 mg GOx were dispersed in 10 mL PBS buffer solution (100 mM, pH 7.0). Then, the GOx solution (5 mg mL⁻¹) was added into PVP solution (10 mg mL⁻¹ in deionized water) at the ratio of 1:1 (v/v), followed by incubation in an ice bag on a shaker. After shaking for 30 min at 200 rpm, the PVP was introduced and finally formed GOx/PVP complexes. Tp (31.5 mg in 10 mL ethanol) and BD (41.5 mg in 10 mL ethanol) were mixed and then the as-prepared GOx/PVP complexes solution was immediately added under magnetic stirring at room temperature for 30 min. The GOx@TpBD precipitation was collected by centrifugation (10000 rpm, 5 min), washed three times with PBS buffer, and stored at 4 °C.

The synthesis of CAT@TpBD was the same as that of GOx@TpBD. The synthesis of GOx@TpPa and CAT@TpPa was the same as that of GOx@TpBD, except that the 41.5 mg BD was replaced with 31.5 mg Pa.

2.2.2. Synthesis of Platinum nanoparticles (Pt NPs) and Pt NPs@TpBD

The Pt NPs were synthesized as follows: 5 mL of chloroplatinic acid (10 mg mL⁻¹) was added into 20 mL of PVP solution (10 mg mL⁻¹ in ethylene glycol). The solution was refluxed at 180 °C for 10 min, then excess acetone was added into resultant black solution to precipitate Pt NPs. Finally, the suspension was centrifuged (8000 rpm, 5 min) and purified with acetone for three times and once with hexane. Pt NPs were dissolved in 5 mL of deionized water and stored at 4 °C for further used.

100 μL of the as-synthesized Pt NPs was firstly diluted into 1.0 mL by deionized water, and then the synthesis of Pt NPs@TpBD was the same as that of GOx@TpBD.

2.2.3. Synthesis of multienzyme cascades EnNBHs

The multienzyme cascades EnNBHs was prepared via the co-entrapment of GOx and HRP within TpBD. The 5 mg GOx and 5 mg HRP were dissolved in 5 ml PBS buffer solution (100 mM, pH 7.0), respectively. Then, 100 μ L GOx solution (1 mg mL⁻¹) and 100 μ L HRP solution (1 mg mL⁻¹) were combined and diluted into 1.0 mL by the deionized water, which was followed by the addition of PVP solution (10 mg mL⁻¹ in deionized water) at the ratio of 1:1 (v/v). Finally, the synthesis of multienzyme cascades EnNBHs was the same as the synthesis of GOx@TpBD.

2.2.4. Synthesis of GOx@ZIF-8

The GOx@ZIF-8 was synthesized by the reported method [12]. 50 mg GOx were dispersed in 10 mL PBS buffer solution (100 mM, pH 7.0). Then, the GOx solution (5 mg mL⁻¹, 2 mL), 184.5 mg Zn (NO₃)₂·6H₂O (dissolved in 2 ml deionized water), and 2052.8 mg 2-MI (dissolved in 20 mL deionized water) were mixed under magnetic stirring for 30 min at room temperature. The GOx@ZIF-8 precipitation was collected by centrifugation (10000 rpm, 5 min), washed three times with PBS buffer, and was stored at 4 °C for further characterization.

2.2.5. Enzyme immobilization efficiency and loading capacity

The enzyme immobilization efficiency and loading capacity were determined by the Bradford method [43]. Briefly, the standard curve was first measured with different concentration of GOx to calculate the free forms in the supernatant. After entrapment, the supernatant was collected and 0.5 mL of supernatant was mixed with 2.5 mL of Coomassie Brilliant Blue G-250. Then, the solution was incubated in the dark for 3 min and characterized by a UV-vis spectrophotometer at 595 nm. The immobilization efficiency was calculated by Equation (1):

$$\text{Immobilization efficiency} = \frac{C_0V_0 - C_1V_1}{C_0V_0} \times 100\% \quad (1)$$

Here, the C_0/V_0 and C_1/V_1 are the initial concentration/volume of GOx added for entrapment and in the supernatant, respectively.

The loading capacity (wt, %) of EnNBHs was calculated by Equation (2):

$$\text{Loading capacity} = \frac{m}{M-m} \times 100\% \quad (2)$$

Here, the M and m are the weight of freeze-dried EnNBHs and enzymes entrapped in EnNBHs, respectively.

2.2.6. Biocatalytic activity assay

The biocatalytic activity of GOx and GOx@TpBD were evaluated through monitoring the production of H₂O₂ (Equation 3 and 4). 100 μL GOx and GOx@TpBD were dispersed into 900 μL PBS buffer solution (100 mM, pH 7.0) containing 100 μL glucose (50 mM), followed by the incubation at 25 °C. 50 μL supernatant, 50 μL TMB solution (1.2 mg mL⁻¹), 50 μL HRP solution (1 mg mL⁻¹), and 850 μL PBS buffer solution (100 mM, pH 7.0) was mixed, and then the absorbance of the generated H₂O₂ at 652 nm was recorded.



The biocatalytic activity of CAT and CAT@TpBD were determined by tracing the decomposition of H₂O₂ (Equation 5). The 100 μL CAT and CAT@TpBD were dispersed into 900 μL PBS buffer solution (100 mM, pH 7.0) containing 200 μL H₂O₂ (0.5 mM), followed by incubated at 25 °C water bath, and then the residual H₂O₂ was measured at 652 nm.



The biocatalytic activity of multienzyme cascades EnNBHs were carried out as follows: the 200 μL GOx-HRP and EnNBHs were dispersed into 800 μL PBS buffer solution (100 mM, pH 7.0) containing 100 μL glucose (50 mM), followed by incubated at 25 °C water bath. 500 μL sulfuric acid (6 M) was added to defined the reaction time and caused the reaction solution to change from blue to yellow, then the 100 μL supernatant was collected and diluted into 1 mL by PBS buffer solution (100 mM, pH 7.0) for measuring absorbance at 450 nm.

Notably, the free enzymes and entrapped enzymes within were equivalent in the biocatalytic

activity assay process.

2.2.7. Stability and recyclability test

For the stability test, the free GOx, GOx@ZIF-8, and GOx@TpBD were incubated in different pH values (4 - 10) for 2 h, different temperatures (30 - 70 °C) for 2 h, light (or with C₃N₄) for 1.5 h, and a series of unfavorable conditions (200 μL biocatalysts (~ 50 μg mL⁻¹), 160 μL PBS buffer solution (100 mM, pH 7.0), and 40 μL trypsin (5 mg mL⁻¹), urea (5 mg mL⁻¹), DMF, acetone) for 6 h. Then, the catalytic reaction was performed to determine the residual activity. The recyclability test was conducted in the total volume of reaction system was fixed to 5 mL, and then checked the H₂O₂ in the supernatant after each run. Thereafter, the EnNBHs particles were placed in the fresh substrate solution for next cycle.

2.2.8. Biocatalytic kinetic parameters measurement

Biocatalytic kinetic parameters was calculated according to the Michaelis-Menten equation (6):

$$\frac{1}{v_0} = \frac{K_m}{v_{\max}} \times \frac{1}{[S]} + \frac{1}{v_{\max}} \quad (6)$$

Here, the v_0 and v_{\max} are initial rate and the maximum rate of biocatalytic conversion. $[S]$ is the different concentration of substrate that was initially added into the reaction system and K_m is the Michaelis-Menten constant. The initial biocatalytic conversion rate was calculated by the kinetic curve in the initial reaction stage. The biocatalytic kinetic parameters (K_m and v_{\max}) were fitted through Michaelis-Menten equation based on a series of v_0 and $[S]$.

The catalyst rate constant was calculated by $k_{\text{cat}} = v_{\max} [E]^{-1}$ ($[E]$ is the concentration of enzyme) and used to evaluate the catalytic ability of biocatalysts. The k_{cat}/K_m represented the biocatalytic efficiency of EnBHs.

2.2.9. Characterizations

Transmission electron microscopy (TEM) images were obtained on a field emission transmission electron microscope (JEM-F200, JEM-2100F). Scanning electron microscopy

(SEM) images were conducted by field emission scanning electron microscope (Regulus 8100). Powder X-ray diffraction (PXRD) patterns were obtained from a Rigaku D/max-2500 V/PC X-ray diffractometer with Cu K α radiation ($\lambda=1.54056 \text{ \AA}$), and data were collected in a range of $5-30^\circ$ (2θ) and at a scan rate of 5° min^{-1} . Fourier transform infrared spectroscopy (FT-IR) was conducted on a Nicolet-6700 with pure KBr as background, and spectra was obtained with $400-4000 \text{ cm}^{-1}$. Confocal laser scanning microscopy (CLSM) image of GOx@TpBD nanoparticles was collected by A1R+. N₂ gas adsorption measurement was performed on Micromeritics ASAP 2020 Accelerated Surface Area and Porosimetry Analyzer. The specific areas were determined using Brunauer-Emmett-Teller (BET) adsorption models, and the pore size distributions were measured using Nonlocal Density Functional Theory (NLDFT) methods. Small-angle X-ray scattering (SAXS) data were collected on Bruker NanoSTAR U SAXS at 50 kV, 0.6 mA, and $\lambda=1.54056 \text{ \AA}$. The ultraviolet-visible (UV-vis) absorbance was measured with Hitachi U-3010.

3. Results and discussion

3.1. Preparation and characterizations of CONs-based EnNBHs

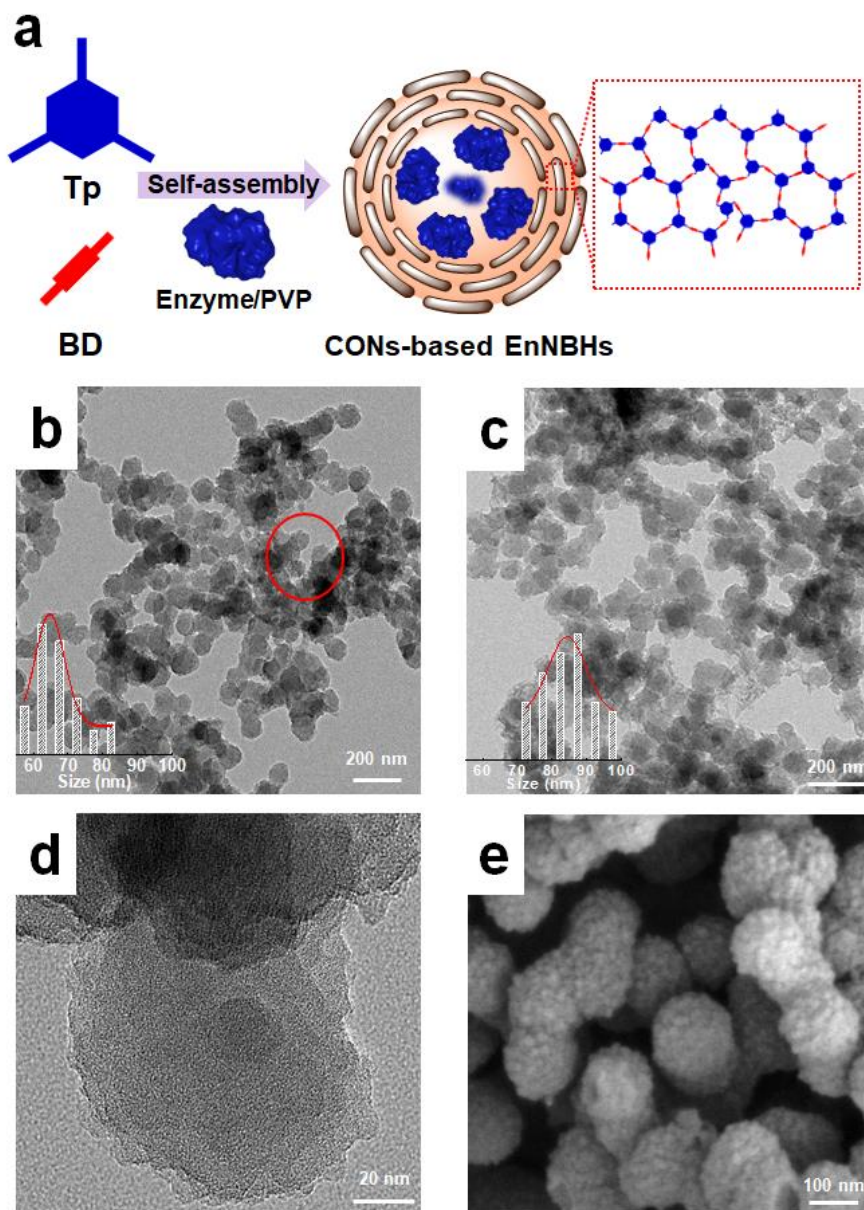


Fig. 1. Synthetic scheme and morphology characterization of CONs-based EnNBHs. (a)

Schematic illustration of the construction of CONs-based EnNBHs. **(b, c)** TEM images of GOx@TpBD obtained after 5 min and 30 min. Insert shows the corresponding particle size distribution. **(d)** TEM image of GOx@TpBD obtained after 5 min at the scale bar of 20 nm. **(e)** SEM image of GOx@TpBD.

The CONs were formed via the Schiff base reaction between aldehyde groups of 1, 3, 5-benzenetricarboxaldehyde (Tp) and amino groups of benzidine (BD) in ethanol/water mixture solution at room temperature. The GOx enzymes were introduced during the *in situ* CONs polymerization to construct GOx@TpBD EnNBHs. The growth process of GOx@TpBD was validated by TEM, which showed that the GOx@TpBD rapidly grew into spherical pellets with the size of ~ 65 nm in 5 min (**Fig. 1(b)**). After 30 min, the size of GOx@TpBD was only slowly increased to ~ 85 nm without obvious shape changes (**Fig. 1(c)**). This indicated that the promoting effect of GOx on the formation of CONs became weaker over time (**Fig. 1(d)** and **(e)**). In contrast, the control system without the addition of GOx (but with PVP) first assembled into amorphous clusters of nanorods in 5 min (**Fig. S1(a)**), and then the nanorods was self-assembly formed spherical pellets but with a few residual nanorods after 30 min (**Fig. S1(b)** and **(c)**). All the evidences proved that GOx indeed showed the ability to promote the nucleation of CONs, thus accelerating the formation of spherical CONs around the proteins.

The chemical and physical structure of TpBD and GOx@TpBD was studied by ^{13}C solid-state nuclear magnetic resonance (NMR) spectroscopy, Fourier-transform infrared spectroscopy (FT-IR), X-ray diffraction (XRD), N_2 -sorption isotherm, and small angle X-ray scattering (SAXS). The ^{13}C NMR spectroscopy was first applied to analyze the formation of TpBD (**Fig. 2(a)**). The absence of the peak at about 190 ppm provided clear evidences for the consumption of Tp building blocks. More imporeantly, the TpBD showed a signal at about 185 ppm, corresponding to the carbonyl carbon of the β -ketoenamine form, and a peak at about 138 ppm was the signal of the formation of new C-N bond [44, 45]. The characteristic peaks of GOx@TpBD were consistent with that of pure TpBD, indicating the local structure was not changed by entrapped enzymes. For GOx@TpBD, the peaks at about 18 and 32 ppm were probably due to the extra methyl group of enzymes [46]. Moreover, the FT-IR spectra exhibited the disappearances of N-H ($3100\text{-}3300\text{ cm}^{-1}$, stretching band of the free BD) and CH=O (2923 cm^{-1} , stretching band of the free Tp),

indicating the occurrence of Schiff-base reaction. Meanwhile, the spectra of TpBD showed extra characteristic bands of C=O (1620 cm^{-1}), C=C (1594 cm^{-1}), aromatic C=C (1458 cm^{-1}), and C-N (1286 cm^{-1}) [46, 47], corresponding to formation of covalent organic networks, which were derived from the β -ketoenamine subunits (**Fig. 2(b)**) [44-46]. The characteristic bands of free GOx appeared at around 1660 cm^{-1} , corresponding to the stretching modes of C=O (amine I band) and 1540 cm^{-1} , corresponding to combination of the stretching modes of C-N and the bending modes of N-H (amine II band), respectively [48]. Notably, the FT-IR spectra of the GOx@TpBD showed that the amine I band intensity of GOx was affected by the strong intensity of C=O (1620 cm^{-1}) of TpBD, albeit only some jagged bands appeared, suggesting the presence of GOx in TpBD [21]. To further demonstrate the entrapment of GOx in TpBD, the energy-dispersive spectrum (EDS) mapping of TEM and confocal laser scanning microscopy (CLSM) were utilized to confirm the distribution of GOx in the CONs. The Sulfur (S) was the exclusive element of GOx and the EDS mapping proved uniform distribution of S elements in the CONs, which was consistent with the distribution of O and N elements, again confirming that the presence of enzymes within the TpBD matrix (Fig. S2). Additionally, the coumarin-labeled GOx were well-dispersed throughout TpBD, suggesting the entrapment of enzyme molecules during the growth of CONs (Fig. S3(a)) [12, 49]. Moreover, this *in situ* entrapment strategy for constructing EnNBHs was further validated by platinum nanoparticles (Pt NPs). In the typical synthesis, the enzymes were replaced with PVP modified Pt NPs ($2 \sim 3\text{ nm}$). The TEM and HAADF-STEM images also showed the distribution of Pt NPs in TpBD, indicating the Pt NPs was entrapped successfully (Fig. S3(b) and (c)). Moreover, the XRD patterns revealed that the Bragg diffraction peaks of simulated TpBD appeared at 3.3° , 6.0° , 11.7° , and 27° , corresponding to (100) (200), (210), and (001) reflection planes, respectively [46, 47]. The diffraction intensity of (100) and (001) reflection planes corresponded to the long-range ordered structure and π - π stacking between the layers, respectively [50]. Notably, compared with simulated TpBD, a shift of the (001)

reflection planes of GOx@TpBD toward lower 2θ values was detected, suggesting the increased stacking distance of adjacent CONs layers. The weakening of the π - π stacking interaction caused a certain random displacement of layers, thereby resulting in the loss of long-range order structure of GOx@TpBD (corresponding to the absence of the first characteristic peak at about 3.3°) and the formation of CONs with short-range order structure (**Fig. 2(c)**) [50]. This short-range order structure was also detected by the TEM (Fig. S4), corresponding to the decrease of (100) reflection planes, which was consistent with the results of XRD pattern. Moreover, the diffraction reflection positions of GOx@TpBD showed a slight shift to low angle, resulting in a larger lattice constant, indicating the existence of more defective structure in GOx@TpBD.

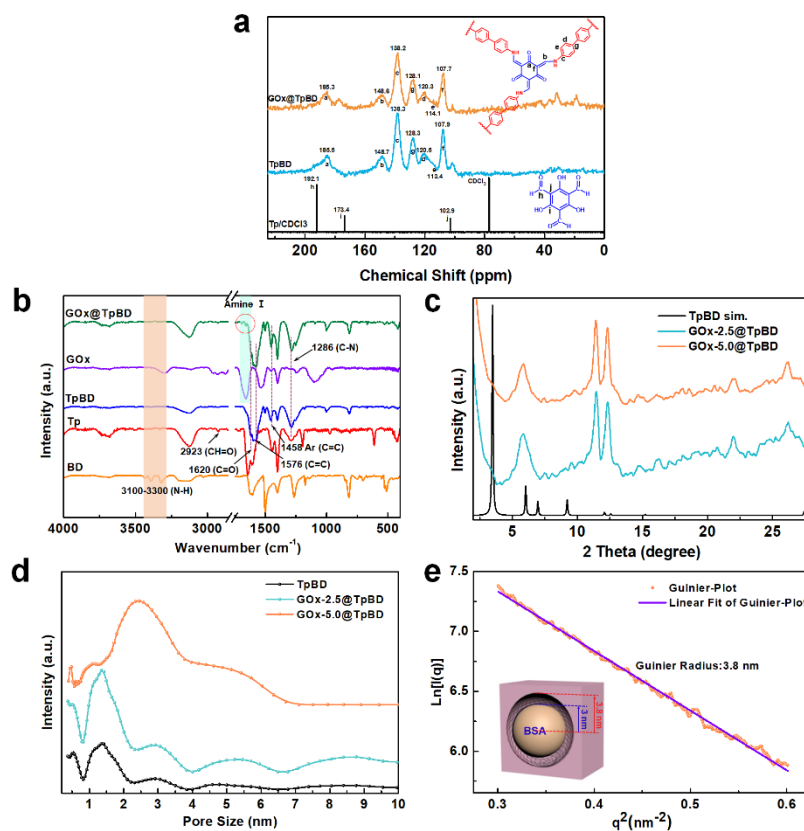


Fig. 2. Structural characterization of EnNBHs. (a) ^{13}C NMR spectra of Tp/ CDCl_3 , TpBD, and GOx@TpBD. (b) FT-IR spectra of BD (orange), Tp (red), TpBD (blue), GOx (purple), and GOx@TpBD (green). (c) XRD pattern of TpBD-COFs, GOx-2.5@TpBD and GOx-5.0@TpBD (GOx-2.5 meaning the introduction of free GOx was 2.5 mg). (d) Pore-size distributions of pure

TpBD, GOx-2.5@TpBD and GOx-5.0@TpBD. (e) SAXS data of the BSA@TpBD. Inset shows the gyration radius of BSA and the observed mesopores in the TpBD.

To investigate whether the change in the amounts of entrapped enzymes could cause the variations of voids, different amounts of GOx (e.g., 2.5 mg, 5.0 mg, 7.5 mg, and 10 mg) were introduced to construct EnNBHs. The immobilization efficiency and loading capacity of EnNBHs were determined by Bradford assay according to a standard calibration curve of GOx (Fig. S5) [43]. When the dosage of GOx was relatively low (less than 7.5 mg), nearly all enzymes could be entrapped in the TpBD particles (Fig. S6). The maximum loading capacity could reach 12.9% (wt %) (Fig. S7), which was higher than many EnNBHs in previous reports (Table S1). In the results of N₂-sorption isotherm, the surface area of pure TpBD was $\sim 82.9 \text{ m}^2 \text{ g}^{-1}$, while the GOx-2.5@TpBD and GOx-5.0@TpBD were $\sim 74.4 \text{ m}^2 \text{ g}^{-1}$ and $\sim 58.8 \text{ m}^2 \text{ g}^{-1}$, respectively (Fig. S8). Notably, compared with pure TpBD, the surface area of GOx@TpBD composites was gradually decreased, which was consistent with the presence of the entrapped enzymes. The pore size distribution was calculated by nonlocal density functional theory (NLDFT) and the pore size of the pure TpBD was about 1.5 nm, which was consistent with the reported TpBD (1.0 \sim 1.7 nm) [46]. However, the GOx@TpBD exhibited a wide pore size distribution ranging from 1 \sim 5 nm (**Fig. 2(d)**). It was then concluded that the formation of mesopores should be arisen from the presence of enzymes. As reported, the size of GOx molecule was about 5.5 nm \times 7 nm \times 8 nm [51], which was much larger than the pore size of GOx@TpBD and TpBD, suggesting that enzymes should be wrapped by TpBD while not shielding the intrinsic pores. To confirm this hypothesis, bovine serum albumin (BSA) was selected as a model protein in this study. The SAXS data revealed that mesopores appeared in BSA@TpBD and the Guinier radius (radius of gyration, R_g) of these mesopores was $\sim 3.8 \text{ nm}$, according to the Unified Model (**Fig. 2(e)**). It was noted that the R_g of BSA was $\sim 3 \text{ nm}$ [52], which was about 30% smaller than that of

BSA@TpBD. Therefore, the mesopores of BSA@TpBD were large enough to accommodate the BSA molecules (**Fig. 2(e)**, inset).

2.2. Protective effect of CONs for EnNBHs

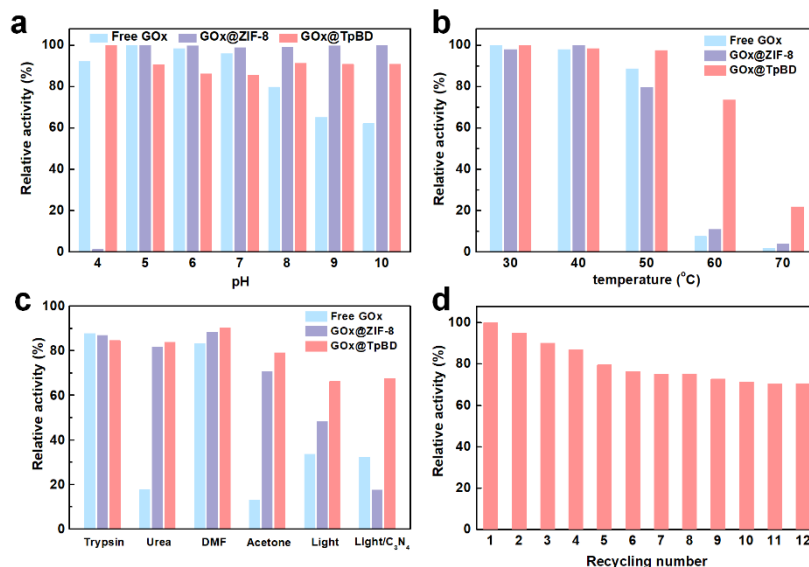


Fig. 3. Stability of EnNBHs against various harsh conditions. (a) pH values, **(b)** Thermal variations, **(c)** Enzyme inhibitors, **(d)** Recycling experiments.

Given the importance of the stability of EnNBHs in practical applications, the protecting effect of the TpBD particles was examined under various inhospitable conditions, including extreme pH values, high temperatures, and in the presence of trypsin, urea, N, N-dimethylformamide (DMF), acetone, and light irradiation (**Fig. 3**). ZIF-8-based EnNBHs was also selected and prepared as a control. After incubating the biocatalysts at pH 4 ~ 10, the GOx@TpBD retained over 85% of its original enzyme activity under either acidic or basic condition, while the enzyme activity of free GOx dramatically decreased to 62% under pH 10 (**Fig. 3(a)**). Notably, GOx@ZIF-8 almost lost all enzyme activity under pH 4, which was attributed to the complete decomposition of ZIF-8 particles under acidic conditions (Fig. S9). These results clearly showed that the TpBD provide better protection for enzymes under a wide range of pH value. Furthermore, GOx@TpBD possessed higher thermal stability than both free GOx and GOx@ZIF-8. GOx@TpBD retained

72% of initial enzyme activity after being exposed to 60 °C for 120 min. In contrast, free GOx and GOx@ZIF-8 retained only ~ 8% and ~ 11% of their initial enzyme activity, respectively (**Fig. 3(b)**). Besides, the stabilities of GOx@TpBD under other denaturing conditions were also examined (**Fig. 3(c)**). After being incubated in acetone for 6 h, the free GOx and GOx@ZIF-8 retained ~ 13% and ~ 70% of their initial enzyme activity, while over 80% enzyme activity was left for GOx@TpBD. Similar results were also observed under the urea-treated experiment. The enzyme-photo-coupled catalysis was an emerging efficient platform in green biomanufacturing, and the stability of biocatalyst under light irradiations or photocatalyst (C₃N₄) was of great importance. Finally, the light was used as a denaturing agent to explore the protection to the biomolecules from CONS-based EnNBHs. Irradiating the biocatalysts with simulated sunlight (Xe lamp) for 90 min, the relative enzyme activity of GOx@TpBD, GOx@ZIF-8 and free GOx were 66%, 48% and 33%, respectively. In addition, when the biocatalysts were incubated with C₃N₄ under light irradiation, the enzyme activity of GOx@ZIF-8 was further reduced to ~ 17% of its original enzyme activity while negligible effect was observed for free GOx and GOx@TpBD (**Fig. 3(c)**). The UV-vis spectra showed the cooperation between C₃N₄ and light could promote the decomposition of ZIF-8 and destroy the Zn-N coordination bond (Fig. S10). The released 2-MI would then denature the GOx and lead to the reduction of enzyme activity.

In addition to the stability, the catalytic kinetics of GOx@TpBD were evaluated. Michaelis-Menten kinetics and the catalytic rate constants (k_{cat}) of free GOx, GOx@TpBD and GOx@ZIF-8 were calculated (Fig. S11(a), (b) and (c)). The K_m of free GOx, GOx@TpBD and GOx@ZIF-8 were 17.29 mM, 29.40 mM, and 37.47 mM, respectively, manifesting that both GOx@TpBD and GOx@ZIF-8 exhibited lower affinity to substrates. The k_{cat} value of GOx@TpBD was calculated to be 84.4 s⁻¹, which was ~ 1.35 times higher than that of GOx@ZIF-8 (62.4 s⁻¹), ascribing to the larger pore apertures of GOx@TpBD (Fig. S11(d)). Specifically, the pore size distribution of GOx@TpBD was 1 ~ 5 nm, which was broader than that of GOx@ZIF-8 (< 2 nm). Therefore,

more substrate molecules could access to active site of GOx rapidly, thus enhancing the reaction rate by GOx@TpBD. In short, two parameters jointly dominate the higher catalytic rate of CONs-based EnNBHs: (1) the facilitated diffusion of reactants caused by the larger voids [53]; (2) the enlarged interfacial contact between enzyme active sites and host materials [15]. The robustness and durability of CONs-based EnNBHs were further investigated. The enzyme activity of GOx@TpBD was decreased during the initial five cycles (**Fig. 3(d)**), possibly due to the loss of small-size particles of EnNBHs during recovery test rather than enzyme leakage (Fig. S12). As last, the versatility of the *in situ* entrapment strategy was further demonstrated in our study. TpPa, another CONs, was employed to entrap GOx and catalase (CAT) and the enzyme activity was assessed. The CAT@TpPa was thermally stable at 30-60 °C with the retention of ~ 60% of initial enzyme activity, while that of the free CAT was dramatically reduced to ~ 2% at 60 °C (Fig. S13 and S14).

2.3. Artificial cell nanoreactor for biocatalysis

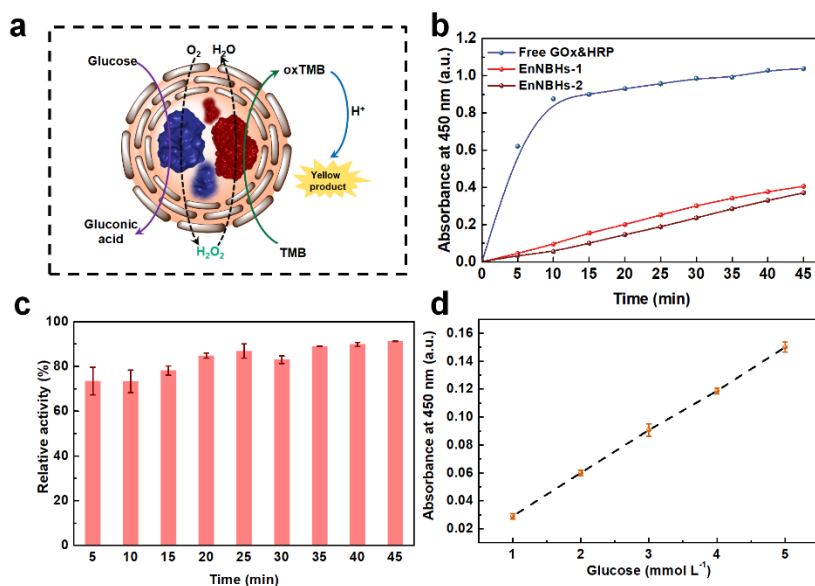


Fig. 4. Enzyme catalytic performance of EnNBHs. (a) Demonstration of the GOx-HRP cascade catalysis in EnNBHs. (b) The enzyme activity of the cascade catalysis of free GOx-HRP, EnNBHs-1, and EnNBHs-2 by measuring UV-vis absorbance at 450 nm. (c) The relative enzyme

activity EnNBHs-1 under different reaction time after storage at 4 °C for 21 days. **(d)** Linear change of UV-vis absorbance at 450 nm in the presence of variable concentrations of glucose.

Multienzyme cascade reactions in cellular environment are nature's powerful chemical transformation processes [54]. Thus, constructing a cell-mimic nanoreactor capable of multienzyme biocatalysis is indispensable in biotechnology and many industrial (bio)chemical processes [55]. Accordingly, we fabricated multienzyme EnNBHs by co-entrapping GOx and HRP in CONs. With the help of GOx, glucose was oxidized into gluconic acid and hydrogen peroxide (H_2O_2). Then, the H_2O_2 generated in the previous step further oxidized 3, 3', 5, 5'-tetramethylbenzidine (TMB) into oxTMB with the assistance of HRP (**Fig. 4(a)**) [28]. The EnNBHs-1 denotes the direct co-entrapment of GOx and HRP, while the EnNBHs-2 denotes the combination of GOx-EnNBHs and HRP-EnNBHs. Compared with free GOx-HRP cascades, the reaction rate of EnNBHs-1 was slower, mainly owing to the hindering effect of the networks of TpBD (**Fig. 4(b)** and S15). By contrast with EnNBHs-1, the relative enzyme activity of EnNBHs-2 could only be increased from ~ 56% to 90% as a function of reaction time (Fig. S16). The enhancement of enzyme cascade activity may be ascribed to the shortened mass transfer distance by co-entrapment (**Fig. 4(b)**) [56-58]. Additionally, the stability of EnNBHs-1 was evaluated by incubation at 4 °C for 21 days. The enzyme activity could retain 80% of its original enzyme activity, indicating the EnNBHs were stable during storage and transportation (**Fig. 4(c)**). The good positive linearities between UV-vis absorbance at 450 nm and variable concentrations of glucose was observed (**Fig. 4(d)**). Combined with the robustness of CONs, it suggested great potential of CONs-based EnNBHs in the area of biobanking or biosensing.

4. Conclusions

In conclusion, we demonstrated a facile yet versatile strategy by *in situ* entrapping biomolecules within CONs for constructing EnNBHs. The *in situ* entrapped enzymes displayed enhanced robustness and durability against various denaturing conditions, including pH

fluctuations, high temperature, organic solvents, urea, acetone, and light irradiation. Furthermore, the hierarchically porous CONs were generated by the entrapped enzymes, which enabled the rapid diffusion of reactants to active site and resulted in the enhancement of enzyme activity of EnNBHs. Overall, our study may provide a generic platform to extend the applications of biomolecules and reticular framework materials via *in situ* entrapment strategy. Considering the rapid advances in reticular chemistry, the possibilities of exploring framework materials to elaborately design EnNBHs seem limitless.

Declaration of Competing Interest

The authors declared that they have no conflict of interest to this work.

Acknowledgement

This work was supported by the National Key R&D Program of China (2021YFC2102300), the National Natural Science Funds of China (22122809), Natural Science Fund of Tianjin (19JCYBJC19700), Royal Society International Collaboration Award (ICA/R1/180317), Open Funding Project of the State Key Laboratory of Biochemical Engineering (2020KF-06), and Tianjin Synthetic Biotechnology Innovation Capacity Improvement Project (TSBICIP-KJGG-003) for financial support.

Supplementary materials

Supplementary material associated with this article can be found, in the online version, at doi:

References

- [1] A. Schmid, J. S. Dordick, B. Hauer, et al., Industrial biocatalysis today and tomorrow, *Nature*, 409 (2001) 258-268.
- [2] R. A. Sheldon, S. van Pelt, Enzyme immobilisation in biocatalysis: why, what and how, *Chem. Soc. Rev.* 42 (2013) 6223-6235.
- [3] J. Liu, Z. Y. Guo, K. Liang, Biocatalytic metal-organic framework-based artificial cells, *Adv. Funct. Mater.* 29 (2019) 1905321.
- [4] Z. Y. Guo, J. J. Richardson, B. Kong, et al., Nanobiohybrids: materials approaches for bioaugmentation, *Sci. Adv.* 6 (2020) eaaz0330.
- [5] J. Y. Liang, K. Liang, Biocatalytic metal-organic frameworks: prospects beyond bioprotective porous matrices, *Adv. Funct. Mater.* 30 (2020) 2001678.
- [6] R. Reshmy, E. Philip, R. Sirohi, et al., Nanobiocatalysts: advancements and applications in enzyme technology, *Bioresour. technol.* 337 (2021) 125491.
- [7] W. B. Liang, P. Wied, F. Carraro, et al., Metal-organic framework-based enzyme biocomposites, *Chem. Rev.* 121 (2021) 1077-1129.
- [8] B. Wang, R. B. Lin, Z. J. Zhang, et al., Hydrogen-bonded organic frameworks as a tunable platform for functional materials, *J. Am. Chem. Soc.* 142 (2020) 14399-14416.
- [9] J. Gan, A. R. Bagheri, N. Aramesh, et al., Covalent organic frameworks as emerging host platforms for enzyme immobilization and robust biocatalysis - a review, *Int. J. Biol. Macromol.* 167 (2021) 502-515.
- [10] M. B. Majewski, A. J. Howarth, P. Li, et al., Enzyme encapsulation in metal-organic frameworks for applications in catalysis, *Crystengcomm*, 19 (2017) 4082-4091.
- [11] S. M. Huang, X. X. Kou, J. Shen, et al., "Armor-plating" enzymes with metal-organic frameworks (MOFs), *Angew. Chem. Int. Edit.* 59 (2020) 8786-8798.
- [12] K. Liang, R. Ricco, C. M. Doherty, et al., Biomimetic mineralization of metal-organic frameworks as protective coatings for biomacromolecules, *Nat. Commun.* 6 (2015) 7240.
- [13] F. J. Lyu, Y. F. Zhang, R. N. Zare, et al., One-pot synthesis of protein-embedded metal-organic frameworks with enhanced biological activities, *Nano Lett.* 14 (2014) 5761-5765.
- [14] F. K. Shieh, S. C. Wang, C. I. Yen, et al., Imparting functionality to biocatalysts via embedding enzymes into nanoporous materials by a de novo approach: size-selective sheltering of catalase in metal-organic framework microcrystals, *J. Am. Chem. Soc.* 137 (2015) 4276-4279.

- [15] F. S. Liao, W. S. Lo, Y. S. Hsu, et al., Shielding against unfolding by embedding enzymes in metal-organic frameworks via a de novo approach, *J. Am. Chem. Soc.* 139 (2017) 6530-6533.
- [16] M. Hu, Y. Ju, K. Liang, et al., Void engineering in metal-organic frameworks via synergistic etching and surface functionalization, *Adv. Funct. Mater.* 26 (2016) 5827-5834.
- [17] S. Gao, J. W. Hou, Z. Y. Deng, et al., Improving the acidic stability of zeolitic imidazolate frameworks by biofunctional molecules, *Chem*, 5 (2019) 1597-1608.
- [18] S. A. Yuan, L. F. Zou, J. S. Qin, et al., Construction of hierarchically porous metal-organic frameworks through linker labilization, *Nat. Commun.* 8 (2017) 15356.
- [19] Y. Y. Sun, J. F. Shi, S. H. Zhang, et al., Hierarchically porous and water-tolerant metal-organic frameworks for enzyme encapsulation, *Ind. Eng. Chem. Res.* 58 (2019) 12835-12844.
- [20] J. Y. Liang, S. Gao, J. Liu, et al., Hierarchically porous biocatalytic MOF microreactor as a versatile platform towards enhanced multienzyme and cofactor-dependent biocatalysis, *Angew. Chem. Int. Edit.* 60 (2021) 5421-5428.
- [21] X. L. Wu, H. Yue, Y. Y. Zhang, et al., Packaging and delivering enzymes by amorphous metal-organic frameworks, *Nat. Commun.* 10 (2019) 5165.
- [22] G. S. Chen, S. M. Huang, X. X. Kou, et al., Embedding functional biomacromolecules within peptide-directed metal-organic framework (MOF) nanoarchitectures enables activity enhancement, *Angew. Chem. Int. Edit.* 59 (2020) 13947-13954.
- [23] C. Hu, Y. X. Bai, M. Hou, et al., Defect-induced activity enhancement of enzyme-encapsulated metal-organic frameworks revealed in microfluidic gradient mixing synthesis, *Sci. Adv.* 6 (2020) eaax5785.
- [24] P. Li, Q. Chen, T. C. Wang, et al., Hierarchically engineered mesoporous metal-organic frameworks toward cell-free immobilized enzyme systems, *Chem*, 4 (2018) 1022-1034.
- [25] M. A. Luzuriaga, R. P. Welch, M. Dharmawardana, et al., Enhanced stability and controlled delivery of MOF-encapsulated vaccines and their immunogenic response in vivo, *ACS Appl. Mater. Inter.* 11 (2019) 9740-9746.
- [26] C. Y. Sun, C. Qin, X. L. Wang, et al., Zeolitic imidazolate framework-8 as efficient pH-sensitive drug delivery vehicle, *Dalton Trans.* 41 (2012) 6906-6909.
- [27] M. Taheri, T. Tsuzuki, Photo-accelerated hydrolysis of metal organic framework ZIF-8, *ACS Mater. Lett.* 3 (2021) 255-260.
- [28] M. M. Li, S. Qiao, Y. L. Zheng, et al., Fabricating covalent organic framework capsules with commodious microenvironment for enzymes, *J. Am. Chem. Soc.* 142 (2020) 6675-6681.
- [29] C. S. Diercks, O. M. Yaghi, The atom, the molecule, and the covalent organic framework, *Science*, 355 (2017)

eaal1585.

- [30] X. Feng, X. S. Ding, D. L. Jiang, Covalent organic frameworks, *Chem. Soc. Rev.* 41 (2012) 6010-6022.
- [31] S. Kandambeth, V. Venkatesh, D. B. Shinde, et al., Self-templated chemically stable hollow spherical covalent organic framework, *Nat. Commun.* 6 (2015) 6786.
- [32] Q. Sun, C. W. Fu, B. Aguila, et al., Pore environment control and enhanced performance of enzymes infiltrated in covalent organic frameworks, *J. Am. Chem. Soc.* 140 (2018) 984-992.
- [33] Q. Sun, B. Aguila, P. C. Lan, et al., Tuning pore heterogeneity in covalent organic frameworks for enhanced enzyme accessibility and resistance against denaturants, *Adv. Mater.* 31 (2019) 1900008.
- [34] G. S. Chen, S. M. Huang, Y. Shen, et al., Protein-directed, hydrogen-bonded biohybrid framework, *Chem*, 7 (2021) 2722-2742.
- [35] J. K. Tang, J. Liu, Q. Z. Zheng, et al., In-situ encapsulation of protein into nanoscale hydrogen-bonded organic frameworks for intracellular biocatalysis, *Angew. Chem. Int. Edit.* 60 (2021) 22315-22321.
- [36] Z. P. Tang, X. Y. Li, L. J. Tong, et al., A biocatalytic cascade in an ultrastable mesoporous hydrogen-bonded organic framework for point-of-care biosensing, *Angew. Chem. Int. Edit.* 60 (2021) 23608-23613.
- [37] D. Beaudoin, T. Maris, J. D. Wuest, Constructing monocrystalline covalent organic networks by polymerization, *Nat. Chem.* 5 (2013) 830-834.
- [38] T. Hasell, A. I. Cooper, Porous organic cages: soluble, modular and molecular pores, *Nat. Rev. Mater.* 1 (2016) 16053.
- [39] Y. W. Gu, J. L. Zhao, J. A. Johnson, Polymer networks: from plastics and gels to porous frameworks, *Angew. Chem. Int. Edit.* 59 (2020) 5022-5049.
- [40] C. J. Lu, T. Ben, S. X. Xu, et al., Electrochemical synthesis of a microporous conductive polymer based on a metal-organic framework thin film, *Angew. Chem. Int. Edit.* 53 (2014) 6454-6458.
- [41] J. Tan, S. Namuangruk, W. F. Kong, et al., Manipulation of amorphous-to-crystalline transformation: towards the construction of covalent organic framework hybrid microspheres with NIR photothermal conversion ability, *Angew. Chem. Int. Edit.* 55 (2016) 13979-13984.
- [42] G. S. Chen, S. M. Huang, X. X. Kou, et al., A convenient and versatile amino-acid-boosted biomimetic strategy for the nondestructive encapsulation of biomacromolecules within metal-organic frameworks, *Angew. Chem. Int. Edit.* 58 (2019) 1463-1467.
- [43] M. M. Bradford, A rapid and sensitive method for the quantitation of microgram quantities of protein utilizing the principle of protein-dye binding, *Anal. Biochem.* 72 (1976) 248-254.

- [44] S. Ghosh, A. Nakada, M. A. Springer, et al., Identification of prime factors to maximize the photocatalytic hydrogen evolution of covalent organic frameworks, *J. Am. Chem. Soc.* 142 (2020) 9752-9762.
- [45] T. Zhou, L. Wang, X. Y. Huang, et al., PEG-stabilized coaxial stacking of two-dimensional covalent organic frameworks for enhanced photocatalytic hydrogen evolution, *Nat. Commun.* 12 (2021) 3934.
- [46] B. P. Biswal, S. Chandra, S. Kandambeth, et al., Mechanochemical synthesis of chemically stable isoreticular covalent organic frameworks, *J. Am. Chem. Soc.* 135 (2013) 5328-5331.
- [47] S. Chandra, S. Kandambeth, B. P. Biswal, et al., Chemically stable multilayered covalent organic nanosheets from covalent organic frameworks via mechanical delamination, *J. Am. Chem. Soc.* 135 (2013) 17853-17861.
- [48] A. Barth, C. Zscherp, What vibrations tell us about proteins, *Q. Rev. Biophys.* 35 (2002) 369-430.
- [49] W. B. Liang, F. Carraro, M. B. Solomon, et al., Enzyme encapsulation in a porous hydrogen-bonded organic framework, *J. Am. Chem. Soc.* 141 (2019) 14298-14305.
- [50] T. Sick, J. M. Rotter, S. Reuter, et al., Switching on and off interlayer correlations and porosity in 2D covalent organic frameworks, *J. Am. Chem. Soc.* 141 (2019) 12570-12581.
- [51] H. J. Hecht, H. M. Kalisz, J. Hendle, et al., Crystal structure of glucose oxidase from *Aspergillus niger* refined at 2.3 angstrom resolution, *J. Mol. Biol.* 229 (1993) 153-172.
- [52] P. Pernot, A. Round, R. Barrett, et al., Upgraded ESRF BM29 beamline for SAXS on macromolecules in solution, *J. Synchrot. Radiat.* 20 (2013) 660-664.
- [53] G. S. Chen, X. X. Kou, S. M. Huang, et al., Modulating the biofunctionality of metal-organic framework-encapsulated enzymes through controllable embedding patterns, *Angew. Chem. Int. Edit.* 59 (2020) 2867-2874.
- [54] W. H. Chen, M. Vazquez-Gonzalez, A. Zoabi, et al., Biocatalytic cascades driven by enzymes encapsulated in metal-organic framework nanoparticles, *Nat. Catal.* 1 (2018) 689-695.
- [55] D. Graefe, J. Gaitzsch, D. Appelhans, et al., Cross-linked polymersomes as nanoreactors for controlled and stabilized single and cascade enzymatic reactions, *Nanoscale*, 6 (2014) 10752-10761.
- [56] W. B. Liang, H. S. Xu, F. Carraro, et al., Enhanced activity of enzymes encapsulated in hydrophilic metal-organic frameworks, *J. Am. Chem. Soc.* 141 (2019) 2348-2355.
- [57] Y. Kim, T. Yang, G. Yun, et al., Hydrolytic transformation of microporous metal-organic frameworks to hierarchical micro- and mesoporous MOFs, *Angew. Chem. Int. Edit.* 54 (2015) 13273-13278.
- [58] J. F. Shi, Y. Z. Wu, S. H. Zhang, et al., Bioinspired construction of multi-enzyme catalytic systems, *Chem. Soc. Rev.* 47 (2018) 4295-4313.